Direct test of defect mediated laser induced melting theory for two dimensional solids

Debasish Chaudhuri* and Surajit Sengupta†
Satyendra Nath Bose National Centre for Basic Sciences,
Block-JD, Sector-III, Salt Lake,Calcutta - 700098.
(Dated: February 2, 2008)

We investigate by direct numerical solution of appropriate renormalization flow equations, the validity of a recent dislocation unbinding theory for laser induced freezing/melting in two dimensions. The bare elastic moduli and dislocation fugacities which are inputs to the flow equations are obtained for three different 2-d systems (hard disk, inverse 12^{th} power and the Derjaguin-Landau-Verwey-Overbeek potentials) from a restricted Monte Carlo simulation sampling only configurations *without* dislocations. We conclude that (a) the flow equations need to be correct at least up to third order in defect fugacity to reproduce meaningful results, (b) there is excellent quantitative agreement between our results and earlier conventional Monte Carlo simulations for the hard disk system and (c) while the qualitative form of the phase diagram is reproduced for systems with soft potentials there is some quantitative discrepancy which we explain.

PACS numbers: 64.70.Dv, 64.60.Ak, 82.70.Dd

I. INTRODUCTION

Examples of phase transitions mediated by the unbinding of defect pairs abound in two dimensions. The quasi-longranged- order to disorder transition in the XY and planar rotor models[1,2], the melting transition of a two dimensional solid[3], the superconductor to normal phase transition in two dimensional Josephson junction arrays[4], the commensurate- incommensurate transition of the striped phase of smectic liquid crystals on anisotropic substrates[5], and the more recent discovery of a defect mediated re-entrant freezing transition in two dimensional colloids in an external periodic potential[6,7] are all understood within such defect unbinding theories. While the very first defect mediated transition theory for the phase transition in the XY-model by Kosterlitz and Thouless (KT)[1] enjoyed almost immediate acceptance and was verified in simulations[2] as well as experiments[8,9], defect mediated theories of two dimensional melting took a long time to gain general acceptance in the community[10]. There were several valid reasons for this reticence however.

Firstly, as was recognized even in the earliest papers[11,12] on this subject, the dislocation unbinding transition, which represents an instability of the solid phase, may always be pre-empted by a first order[13,14] transition from a metastable solid to a stable liquid. Whether such a first order melting transition actually occurs or not depends on the temperature of instability T_{KT}; so that if the transition temperature $T_c < T_{KT}$ the unbinding of dislocations does not occur. Clearly, neither this condition nor its converse can hold for all 2d systems in general since T_{KT} is a non-universal number which depends on the "distance" in coupling parameter space between the bare and the fixed point Hamiltonian and hence on the details of the interaction. Secondly, the renormalization group flow equations derived in all defect mediated theories to date are perturbative expansions in the defect density (fugacity) in the ordered phase. How fast does this perturbation series converge? Again, the answer lies in the position of the bare Hamiltonian in the coupling parameter space. For the planar rotor model[1,2], past calculations show that next to leading order terms in the flow equations are essential to reproduce the value of the transition temperature obtained in simulations[2]. Thirdly, defect mediated transitions predict an essential singularity[1] of the correlation length at the transition temperature. This means that effects of finite size[15] would be substantial and may thoroughly mask the true thermodynamic result. A rapid increase of the correlation length also implies that the relaxation time diverges as the transition temperature is approached – critical slowing down. For the two dimensional solid, this last effect is particularly crucial since, even far from the transition, the motion of defects is mainly thermally assisted and diffusional and therefore slow. The equilibration of defect configurations[16] is therefore often an issue even in solids of macroscopic dimensions.

On the other hand, over the last few years it has been possible to test quantitatively some of the non-universal predictions of defect mediated theories of phase transitions using simulations of restricted systems[2,3,17]. A simulation of a system without defects is used to obtain the values for the bare coupling constants which are then taken as inputs to the renormalization group equations for the appropriate defect unbinding theory to obtain quantities like the transition temperature. Needless to say, the simulated system does not undergo a phase transition and therefore problems typically related to diverging correlation lengths and times do not occur. Numerical agreement of the result of this calculation with that of unrestricted simulations or experiments is proof of the validity of the RG flow equations[1,3,11,12]. This

*debc@bose.res.in
†surajit@bose.res.in

idea has been repeatedly applied in the past to analyze defect mediated phase transitions in the planar rotor model[2], two dimensional melting of hard disks[3] and the re-entrant freezing of hard disks in an external periodic potential[17,18]. The last system is particularly interesting in view of its close relation with experiments on laser induced re-entrant freezing transition in charge stabilized colloids[6,7] and this constitutes the subject of the present paper as well.

In this paper we show in detail how restricted simulations of systems of particles interacting among themselves via a variety of interactions and with a commensurate external periodic potential can be used to obtain phase diagrams showing the re-entrant freezing transition. The results obtained are compared to earlier unrestricted simulations for the same systems. Briefly our results are as follows. Firstly, we observe that, as in an earlier study of the planar rotor model[2], next to leading order corrections to the renormalization flow equations are *essential* to reproduce even the gross features of the phase diagram. Specifically, the re-entrant portion of the phase diagram can be reproduced *only* if such correction terms are taken into account. Secondly while we find almost complete agreement with earlier results for the hard disk system which has been studied most extensively, our phase diagram for the other forms of interaction is shifted with respect to the results available in the literature. This may mean either of two things — inadequacy of the RG theory used by us or finite size effects in the earlier results. Lastly, as a by product of our calculations, we have obtained the core energy for defects (dislocations) in these systems and studied its dependence on thermodynamic and potential parameters.

The problem of re-entrant freezing transition of a system of interacting colloidal particles in a periodic potential has an interesting history involving experiments[6,7], simulations[19,20,21,22,23,24,25,26] and theory[27,28]. In last couple of decades soft systems like colloids have been studied extensively[29] both for their own sake and as typical toy models to study various important condensed matter questions like structural and phase transitions through experiments that allow real space imaging. Charged colloids confined within two glass plates form a model 2-d system as the electrostatic force from the plates almost completely suppresses the fluctuations of colloids perpendicular to the plates, practically confining them to a 2-d plane. In their pioneering experiment Chowdhury[6] *et. al.* imposed a simple static background potential which is periodic in one direction and constant in the other (except for an overall Gaussian profile of intensity- variation) by interfering two laser beams. This potential immediately induces a density modulation in the colloidal system. The potential minima are spaced to overlap with the close packed lines of the ideal lattice of the colloidal system at a given density. With increase in potential strength such a colloidal liquid has been observed to solidify. This is known as laser induced freezing (LIF). In a recent experiment[7] it has been shown that with further increase in potential strength, surprisingly, the solid phase re-melts to a modulated liquid. This phenomenon is known as re-entrant laser induced freezing (RLIF). Qualitatively, starting from a liquid phase, the external periodic potential immediately induces a density modulation, reducing fluctuations which eventually leads to solidification. Further increase in the amplitude of the potential reduces the system to a collection of decoupled 1-d strips. The dimensional reduction now *increases* fluctuations remelting the system.

The early mean field theories, namely, Landau theory[6] and density functional theory[27] predicted a change from a first order to continuous transition with increase in potential strength and failed to describe the re-entrant behavior, a conclusion seemingly confirmed by early experiments[6] and some early simulations[19]. Overall, the results from early simulations remained inconclusive however, while one of them[19] claimed to have found a tricritical point at intermediate laser intensities and reentrance, later studies refuted these results[20,21,22]. All of these studies used the change in order parameter and the maximum in the specific heat to identify the phase transition points. While the later studies[20,21,22] found RLIF for hard disks they reported laser induced freezing and absence of any re-entrant melting for the DLVO potential[22] in direct contradiction to experiments[7].

Following the defect mediated disordering approach of Kosterlitz and Thouless[1](KT), Frey, Nelson and Radzihovsky[28](FNR) proposed a detailed theory for the re-entrant transition based on the unbinding of dislocations with Burger's vector parallel to the line of potential minima. This theory predicted RLIF and no tricritical point. The results of this work were in qualitative agreement with experiments[7] and provided a framework for understanding RLIF in general. More accurate simulation studies on systems of hard disks[23], soft disks[25,26], DLVO[24] etc. confirmed the re-entrant freezing-melting transition in agreement with experiments[7] and FNR theory[28]. In these studies the phase transition point was found from the crossing of Binder-cumulants[30,31] of order parameters corresponding to translational and bond- orientational order, calculated for various sub- system sizes. A systematic finite size scaling analysis[23] of simulation results for the 2-d hard disk system in a 1-d modulating potential showed, in fact, several universal features consistent with the predictions of FNR theory. It was shown in these studies that the resultant phase diagram remains system size dependent and the cross- over to the zero field KTHNY melting[11,12] plays a crucial role in understanding the results for small values of the external potential. While the data collapse and critical exponents were consistent with KT theory for stronger potentials, for weaker potentials they match better with critical scaling[23]. A common problem with all the simulation studies might be equilibration with respect to dislocation movements along climb (or even glide) directions. Also, non universal predictions, namely the phase diagram are difficult to compare because the FNR approach

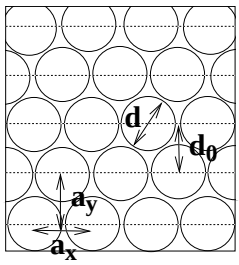

FIG. 1: This cartoon shows a typical 2-d system under consideration. d is the length scale over which repulsive two body potentials are operative. The dashed lines indicate minima of external modulating potential $\beta V(y) = -\beta V_0 \cos(2\pi y/d_0)$. $a_x = a_0$ is the lattice parameter fixed by the density ρ and a_y indicate the average separation between two layers along y-direction perpendicular to a set of close-packed planes. For a perfect triangular lattice $a_y = \sqrt{3}a_0/2$. The modulating potential is commensurate with the lattice such that $d_0 = a_y$.

(like KT theory) is expressed in terms of the appropriate elastic moduli which are notoriously time-consuming to compute near a continuous phase transition. Diverging correlation lengths and times near the phase transition point further complicate an accurate evaluation of the non universal predictions of the theory.

We calculate the phase diagrams of three different 2-d systems with a 1-d modulating potential (see Fig. 1) following the technique of restricted Monte Carlo simulations[2,3,17], to be discussed below. For the laser induced transition we use this method to generate whole phase diagrams. We reject Monte Carlo moves which tend to distort an unit cell in a way which changes the local connectivity[3]. The percentage of moves thus rejected is a measure of the dislocation fugacity[3]. This, together with the elastic constants of the dislocation free lattice obtained separately, are our inputs (bare values) to the renormalization flow equations[28] to compute the melting points and hence the phase diagram. Our results (Fig. 10,12,11) clearly show a modulated liquid (ML) $\rightarrow$ locked floating solid (LFS) $\rightarrow$ ML re-entrant transition with increase in the amplitude (V_0) of the potential. In general, we find, the predictions of FNR theory to be valid.

In section II we first briefly discuss the FNR theory and then go on to show in detail the restricted simulation scheme used by us to obtain the various quantities required to calculate the phase diagram. In section III we give the simulation results. We describe, in detail, the various quantities leading to the phase diagram for one of the systems, viz. the hard disks[3,32]. Then we present the phase diagrams for the other two systems we study. We compare our results with earlier simulations. Lastly, in section IV we summarize our main results and conclude.

II. METHOD

A cartoon corresponding to the systems considered for our study is given in Fig. 1. The elastic free energy of the solid is given in terms of the spatial derivatives of the displacement field $\vec{u}(\vec{r}) = \vec{r} - \vec{r}_0$ with $\vec{r}_0$ being the lattice vectors of the undistorted reference triangular lattice. For a solid in presence of a modulating potential $\beta V(y)$ (Fig. 1) the displacement mode u_y becomes massive, leaving massless u_x modes. After integrating out the u_y modes the free energy of the LFS may be expressed in terms of gradients of u_x and elastic moduli[28], namely, the Young's modulus $K(\beta V_0, \rho)$ and shear modulus $\mu(\beta V_0, \rho)$,

$$\mathcal{H}_{el} = \int dxdy \left[\frac{1}{2}K\left(\frac{\partial u_x}{\partial x}\right)^2 + \frac{1}{2}\mu\left(\frac{\partial u_x}{\partial y}\right)^2\right] \qquad (1)$$

Similar arguments[28] show that among the three sets of low energy dislocations available in the 2-d triangular lattice, only those (type I) with Burger's vector parallel to the line of potential minima survive at large βV_0. Dislocations with Burger's vector pointing along the other two possible close-packed directions (type II) in the 2-d triangular lattice have larger energies because the surrounding atoms are forced to ride the crests of the periodic potential[28]. Within this set of assumptions, the system therefore shares the same symmetries as the XY model. Indeed, a simple rescaling of $x \rightarrow \sqrt{\mu}x$ and $y \rightarrow \sqrt{K}y$ leads this free energy to the free energy of the XY-model with spin-wave stiffness $K_{xy} = \sqrt{K\mu}a_0^2/4\pi^2$ and spin angle $\theta = 2\pi u_x/a_0$:

$$\mathcal{H}_{el} = \int dxdy \ \left[\frac{1}{2}K_{xy}(\nabla\theta)^2\right]$$

This immediately leads to the identification of a vortex in XY model ($\oint d\theta = 2\pi$) with a dislocation of Burger's vector $\vec{b} = \hat{i}a_0$ ($\oint du_x = a_0$, $\hat{i}$ = unit vector along x- direction) parallel to the potential minima *i.e.* the dislocation of type I. The corresponding theory for phase transitions can then be recast as a KT theory[1] and is described in the framework of a two parameter renormalization flow for the spin-wave stiffness $K_{xy}(l)$ and the fugacity of type I dislocations $y'(l)$, where l is a measure of length scale as $l = \ln(r/a_0)$, r being the size of the system. The flow equations are expressed in terms of $x' = (\pi K_{xy} - 2)$ and $y' = 4\pi\ exp(-\beta E_c)$ where E_c is the core energy of type I dislocations which is obtained from the dislocation probability[3,33]. Keeping upto next to leading order terms in y' the renormalization group flow equations[2,34] are,

$$\begin{aligned}\frac{dx'}{dl} &= -y'^2 - y'^2x' \\ \frac{dy'}{dl} &= -x'y' + \frac{5}{4}y'^3. \end{aligned} \qquad (2)$$

Flows in l generated by the above equations starting from initial or "bare" values of x' and y' fall in two categories. If, as $l \to \infty$, y' diverges, the thermodynamic phase is disordered (i.e. ML), while on the other hand if y' vanishes, it is an ordered phase (a LFS)[28]. The two kinds of flows are demarcated by the *separatrix* which marks the phase transition point. For the linearized equations, that keeps upto only the leading order terms in y', the separatrix is simply the straight line $y' = x'$, whereas for the full non-linear equations one needs to calculate this numerically[2,3,34].

The bare numbers for x' and y' are relatively insensitive to system size since our Monte Carlo simulation does not involve a diverging correlation length associated with a phase transition. This is achieved as follows[2,3]. We monitor individual random moves of the particles in a system and look for distortions of the neighboring unit cells. If in any of these unit cells the length of a next nearest neighbor bond becomes smaller than the nearest neighbor bond, the move is rejected. All such moves generate disclination quartets and are shown in the Fig. 2. Notice that each of these moves break a nearest neighbour bond to build a new next nearest neighbour bond, in the process generating two 7-5 disclination pairs. These are the moves rejected in the restricted simulation scheme we follow. The probabilities of such bond breaking moves are however computed by keeping track of the number of such rejected moves. One has to keep track of all the three possible distortions of the unit rhombus with measured probabilities $P_{mi}, i = 1, 3$ (see Fig. 2). Each of these distortions involves four $7-5$ disclinations *i.e.* two possible dislocation- antidislocation pairs which, we assume, occur independently. For a free ($V_0 = 0$) two dimensional system dislocation core energy E_c^t can be found through the relation[33]

$$\Pi = \exp(-\beta\ 2E_c^t) Z(\tilde{K}) \tag{3}$$

where $\Pi = \sum_{i=1}^{3} P_{mi}$ and $Z(\tilde{K})$ is the "internal partition function" incorporating all three types of degenerate orientations of dislocations,

$$Z(\tilde{K}) = \frac{2\pi\sqrt{3}}{\tilde{K}/8\pi - 1} \left(\frac{r_{min}}{a_0}\right)^{2-\tilde{K}/4\pi} I_0\left(\frac{\tilde{K}}{8\pi}\right) \exp\left(\frac{\tilde{K}}{8\pi}\right)$$

where I_0 is a modified Bessel function, $\tilde{K} = \beta K a_0^2$ is a dimensionless Young's modulus renormalized over phonon modes, a_0 being the lattice parameter and r_{min} is the separation between dislocation-antidislocation above which one counts the pairs. The above expression for $Z(\tilde{K})$ and Eq.(3) have been used previously in simulations[3,33] of phase transitions of 2-d systems in absence of any external potential to find the dislocation core energy E_c^t.

The probabilities for occurrence of the dislocation pairs of a specific type themselves P_{di} (Fig. 3) which are proportional to the square of the fugacities, can be computed easily. The probability of dislocation pairs of type I is $P_{d1} = \frac{1}{2}(P_{m2} + P_{m3} - P_{m1})$ and that of type II is $P_{d2} = \frac{1}{4}(P_{m1} + P_{m2} + P_{m3} - 2P_{d1}) = P_{m1}/2$. The validity of the above expressions can be clearly seen from Fig.2.

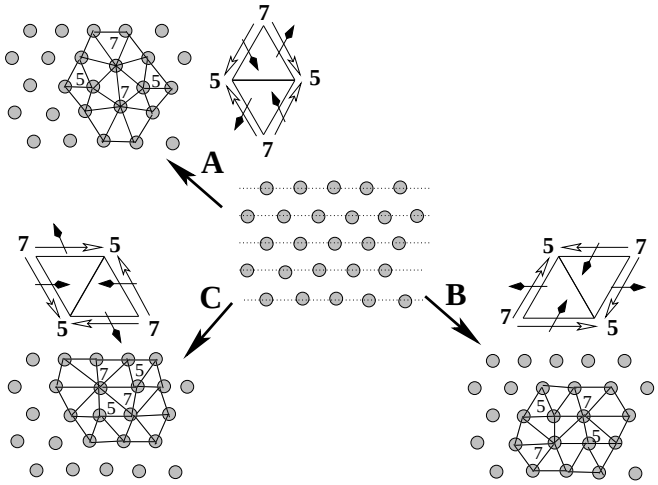

FIG. 2: This diagram depicts all the possible dislocation generating moves that we reject. Starting from the triangular lattice shown in the centre (the dotted lines show the potential minima), in all, there can be three types of dislocation- pair generating moves shown as A, B & C. The numbers 7 and 5 denote the positions of two types of disclinations having seven nearest neighbours and five nearest neighbours respectively. Only those bonds, which are necessary to show distortions due to the generation of disclination quartets, have been drawn. The rhombi near each of the distorted lattice denote the unit cells and open arrows from $7 \to 5$ show the direction of dislocation generating moves. The probabilities of these moves are P_{m1}(A), P_{m2}(B) and P_{m3}(C). Corresponding Burger's vectors (filled arrows) are bisectors pointing towards a direction rotated counter-clockwise starting from $7 \to 5$ directions and are parallel to one of the lattice planes. Notice, the separation between Burger's vectors of a pair along the glide direction (parallel to the Burger's vectors) is a single lattice separation (a_0) and within this construction it is impossible to draw Burger's loop that can generate non-zero Burger's vector. Depending on which of the two possible disclination pairs separate out any one dislocation- antidislocation pair will be formed.

An argument following the lines of Fisher *et. al.*[33] shows that the dislocation probability (number density of dislocation pair per unit cell) for our system,

$$P_{d1} = \exp(-\beta\ 2E_c) Z(\tilde{K}_{xy}) \tag{4}$$

where $2E_c$ is the core energy and $Z(\tilde{K}_{xy})$ is the internal partition function of dislocation pair of type I (single orientation).

$$\begin{aligned} Z(\tilde{K}_{xy}) &= \int_{r>r_{min}} \frac{d^2r}{A_c} \exp\left[-2\pi\tilde{K}_{xy} \log\left(\frac{r}{a_0}\right)\right] \\ &= \frac{2\pi}{\sqrt{3}} \frac{(r_{min}/a_0)^{2-2\pi\tilde{K}_{xy}}}{\pi\tilde{K}_{xy} - 1} \end{aligned} \tag{5}$$

with $\tilde{K}_{xy} = \beta K_{xy}$ and $A_c = \sqrt{3}a_0^2/2$ being the area of an unit cell in the undistorted lattice. We choose $r_{min} = 2a_0$. At this point this choice is arbitrary. We give the detailed reasoning for this choice at the end of section III. Eq.4 and Eq.5 straightaway yield the required core energy E_c. The corresponding fugacity contribution to RG flow equations (Eq.2) is given via

$$y' = 4\pi\sqrt{P_{d1}/Z(\tilde{K}_{xy})} \tag{6}$$

In the above, the following assumption is, however, implicit. Once a nearest neighbor bond breaks and a potential dislocation pair is formed, they separate with probability one[35]. This assumption goes into the identity Eq.4 as well as in Eq.3[3]. Taking the rejection ratios due to bond- breaking as the dislocation probabilities, as well, require this assumption[36].

The same restricted Monte Carlo simulation can be used to find out the stress tensor, and the elastic moduli from the stress-strain curves. The dimensionless stress tensor for a free ($V_0 = 0$) system is given by[37],

$$\beta\sigma_{\lambda\nu}\mathrm{d}^2 = -\frac{\mathrm{d}^2}{S}\left(-\sum_{<ij>}\left\langle\beta\frac{\partial\phi}{\partial r^{ij}}\,\frac{r^{ij}_\lambda r^{ij}_\nu}{r^{ij}}\right\rangle + N\delta_{\lambda\nu}\right) \tag{7}$$

where i, j are particle indices and λ, ν denote directions x, y; $\phi(r^{ij})$ is the two- body interaction, S/d^2 is the dimensionless area of the simulation box[38].

III. RESULTS AND DISCUSSION

In this section we present the calculation of the phase diagram for three different 2-d systems, namely hard disks, soft disks and a system of colloidal particles interacting via the DLVO (Derjaguin-Landau-Verwey-Overbeek)[39,40] potentials. We discuss, first, the calculation of the phase diagram for a two dimensional system of hard disks, in detail. The bulk system of hard disks where particles i and j, in 2-d, interact via the potential $\phi(r^{ij}) = 0$ for $r^{ij} > \mathrm{d}$ and $\phi(r^{ij}) = \infty$ for $r^{ij} \leq \mathrm{d}$, where d is the hard disk diameter and $r^{ij} = |\mathbf{r}^j - \mathbf{r}^i|$ the relative separation of the particles, is known to melt[3,32,41,42,43] from a high density triangular lattice to an isotropic liquid with a narrow intervening hexatic phase[3,11,12,32]. The hard disk free energy is entirely entropic in origin and the only thermodynamically relevant variable is the number density $\rho = N/V$ or the packing fraction $\eta = (\pi/4)\rho\mathrm{d}^2$. Simulations[32], experimental[29] and theoretical[44] studies of hard disks show that for $\eta > .715$ the system exists as a triangular lattice which transforms to a liquid below $\eta = .706$. The small intervening region contains a hexatic phase predicted by the KTHNY theory[11,12] of 2-d melting. Apart from being easily accessible to theoretical treatment[45], experimental systems with nearly "hard" interactions viz. sterically stabilized colloids[29] are available.

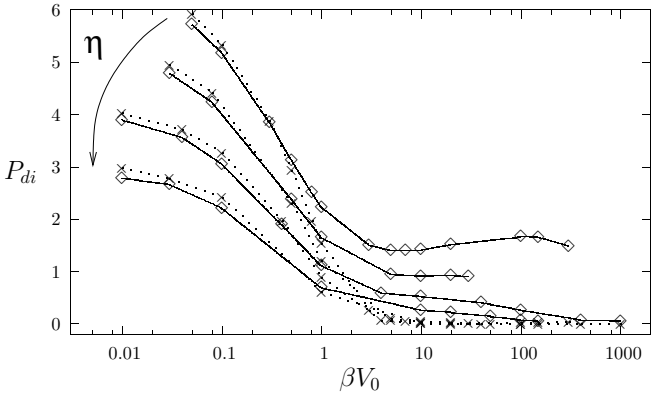

FIG. 3: In this plot the ◇ symbols correspond to P_{d1}, the probability for type I dislocations and the × symbols to P_{d2} the probability for type II dislocations obtained from the P_{mi} (see text and Fig.2) for various η values, arrow denoting the direction of increasing $\eta(= .69, .696, .7029, .71)$. P_{di} for $i = 1, 2$ are expressed in units of 10^4. These probabilities are plotted against the potential strength βV_0. Note that for $\beta V_0 > 1$, the probability for type I dislocations is larger than that of type II. The dots and solid lines are only guides to eye.

In presence of a periodic external potential, the only other energy scale present in the system is the relative potential[46] strength βV_0. If the modulating potential is commensurate with the spacing between close- packed lines, the elastic free energy of this system in it's solid phase follows Eq.1 and the corresponding renormalization flow equations are given by Eq.2.

We obtain the bare y' and x' from Monte Carlo simulations of $43 \times 50 = 2150$ hard disks and use them as initial values for the numerical solution of Eqs. (2). The Monte Carlo simulations for hard disks is done in the usual[47] way viz. we perform individual random moves of hard disks after checking for overlaps with neighbours. When a move is about to be accepted, however, we look for the possibility of bond breaking as described in the previous section (Fig.2). We reject any such move and the rejection ratios for specific types of bond breaking moves give us the dislocation probabilities of type I and II, separately (Fig.3). From Fig.3 it is clear that the probability of type II dislocations *i.e.* P_{d2} drops down to zero for all packing fractions at higher potential strengths βV_0. The external potential suppresses formation of this kind of dislocations. For small βV_0 on the other hand, the probabilities of type I and type II dislocations are roughly the same. This should be a cause of concern since we neglect the contribution of type II dislocations for *all* βV_0. We comment on this issue later in this section.

Using Eq.6 and Eq.5 along with the identity $r_{min} = 2a_0$ gives us the initial value y'_0 to be used in renormalization flow Eq.2 provided we know $\tilde{K}_{xy}$. Again K_{xy} gives x' straightaway. To obtain that we need to calculate the

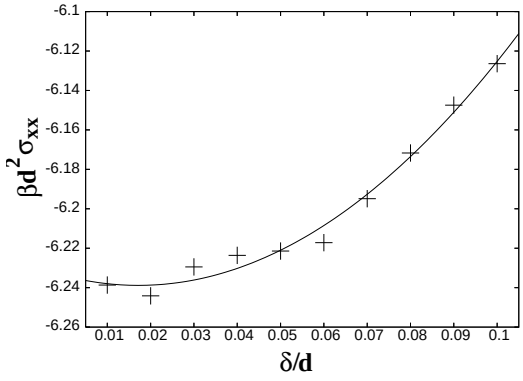

FIG. 4: Plot of $\beta d^2\sigma_{xx}$ vs. δ/d at a strain value $\epsilon_{xx} = .02$ for packing fraction $\eta = .7029$ and potential strength $V_0 = 1$. A second order polynomial fit (solid line) gives $\lim_{\delta\to 0} \beta d^2\sigma_{xx} = -6.23$.

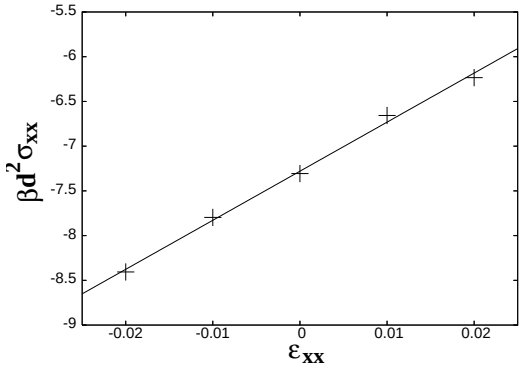

FIG. 5: A typical stress-strain curve used to obtain the Young modulus from a linear fit (solid line). The graph is plotted at $\eta = .7029,\ V_0 = 1.0$. The fitted Young's modulus $\beta K \mathrm{d}^2 = 54.84$.

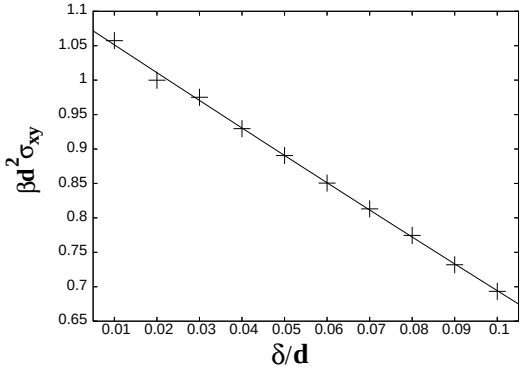

FIG. 6: Plot of $\beta d^2\sigma_{xy}$ vs. δ/d at strain value $\epsilon_{xy} = .08$ at the packing fraction $\eta = .7029$ and potential strength $V_0 = 1$. A second order polynomial fit (solid line) gives $\lim_{\delta\to 0} \beta d^2\sigma_{xy} = 1.092$.

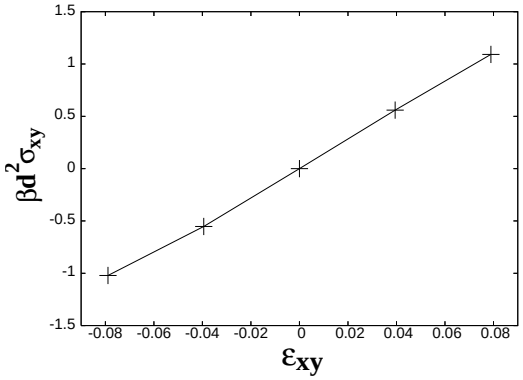

FIG. 7: A typical stress-strain curve used to obtain shear modulus from a linear fit (solid line). The graph is plotted at $\eta = .7029,\ V_0 = 1.0$. The fitted shear modulus $\beta\mu \mathrm{d}^2 = 13.53$.

Young modulus K and shear modulus μ.

Let us again go back to Eq.7, the expression for stress tensor. For hard disk potentials the derivative $\partial\phi/\partial r^{ij}$ becomes a Dirac delta function and the expression for stress can be recast into[37]

$$\beta\sigma_{\lambda\nu}\mathrm{d}^2 = -\frac{\mathrm{d}^2}{S}\left(\sum_{<i,j>}\left\langle \frac{r_\lambda^{ij} r_\nu^{ij}}{r^{ij}}\delta(r^{ij}-d)\right\rangle + N\delta_{\lambda\nu}\right) \tag{8}$$

The presence of Dirac delta function $\delta(r^{ij} - d)$ in the above expression requires that the terms under the summation contribute, strictly, when two hard disks touch each other *i.e.* $r^{ij} \equiv r = \sigma$. In practice, we implement this, by adding the terms under summation when each pair of hard disks come within a small separation $r = \sigma + \delta$. We then find $\beta\sigma_{\lambda\nu}\mathrm{d}^2$ as function of δ and fit the curve to a second order polynomial. Extrapolating to the $\delta \to 0$ limit obtains the value of a given component of stress tensor at each strain value $\epsilon_{\lambda\nu}$[37].

For completeness, now we show how we calculate the two relevant stress-tensors : σ_{xx} at a given longitudinal strain ϵ_{xx} in Fig. 4 and σ_{xy} for a shear strain ϵ_{xy} in Fig. 6. We thus calculate the stress at each value of strain and from the slopes of stress-strain curves find out the bare Young-modulus $\beta K\mathrm{d}^2$ (Fig. 5) and shear-modulus $\beta\mu\mathrm{d}^2$(Fig. 7). To obtain the relevant elastic moduli we give first an elongational strain in x- direction which is parallel to the direction of potential minima to obtain K and subsequently a shear in the same direction to obtain μ. Any strain that forces the system to ride potential hills will give rise to massive displacement modes which do not contribute to elastic theory.

From these elastic moduli we get the 'bare' K_{xy} (and hence $x_0' = \pi K_{xy} - 2$, see section II). This is also required to complete the computation of y_0'. In Fig. 8 we have plotted x_0' and y_0' the bare values of x' and y' for various potential strengths βV_0 at packing fraction $\eta = .7029$ along with the separatrices for the linearized and the non-linear flow equations (Eq. 2). The line of

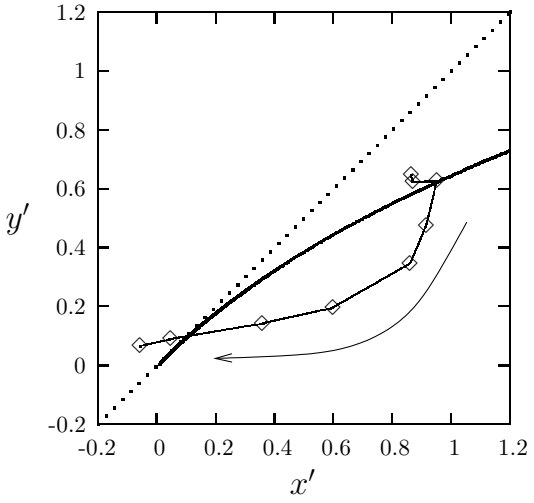

FIG. 8: The initial values of x' and y' obtained from the elastic moduli and dislocation probability at $\eta = .7029$ plotted in $x' - y'$ plane. The line connecting the points is a guide to eye. The arrow shows the direction of increase in $\beta V_0 (= .01, .04, .1, .4, 1, 4, 10, 40, 100)$. The dotted line denotes the separatrix ($y' = x'$) incorporating only the leading order term in KT flow equations. The solid curve is the separatrix when next to leading order terms are included. In $l \to \infty$ limit any initial value below the separatrix flows to $y' = 0$ line whereas that above the separatrix flows to $y' \to \infty$. The intersection points of the line of initial values with the separatrix gives the phase transition points. The plot shows a freezing transition at $\beta V_0 = .1$ followed by a melting at $\beta V_0 = 30$.

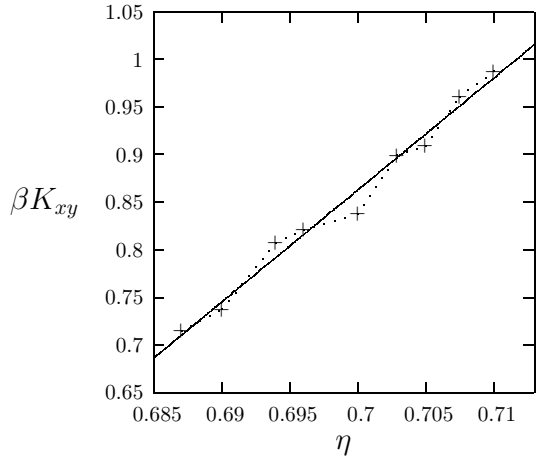

FIG. 9: For hard disk system βK_{xy} varies linearly with η. Data plotted at $V_0 = 1$. The solid line is a linear fit to the form $f(x) = a + bx$ with $a = -7.37$ and $b = 11.76$. At each V_0 the error in K_{xy} determines the error in η: $\delta\eta/\eta = |1 + a/\eta b|(\delta K_{xy}/K_{xy})$.

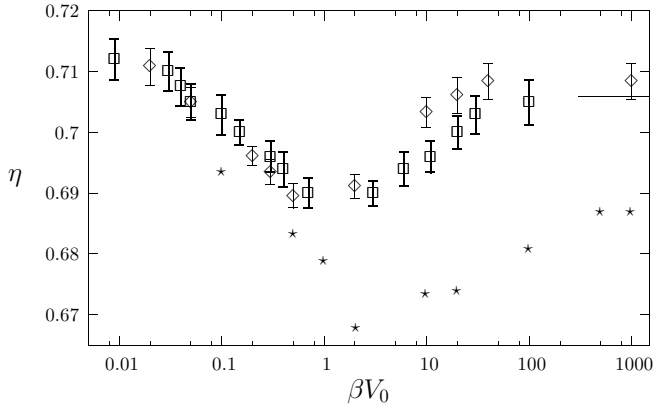

FIG. 10: The phase diagram of the hard disk system in the presence of a 1-d, commensurate, periodic potential in the packing fraction (η) - potential strength (βV_0) plane. The points denoted by $\Box$ correspond to our RG calculation using the techniques described in this paper. The points denoted by $\diamond$[23] and $*$[22] are taken from earlier simulations. The vertical bars denote estimate of error. Our data clearly matches with Ref[7].The horizontal line at $\eta = .706$ denotes the calculated asymptotic phase transition point at $\beta V_0 = \infty$.

initial conditions is seen to cross the non-linear separatrix twice (signifying re-entrant behaviour) while crossing the corresponding linearized separatrix only once at high potential strengths. The phase diagram (Fig. 10) is obtained by computing the points at which the line of initial conditions cut the non-linear separatrix using a simple interpolation scheme. It is interesting to note that within a linear theory the KT flow equations *fail to predict a RLIF transition*. Performing the same calculation for different packing fractions η we find out the whole phase diagram of RLIF in the η- βV_0 plane.

The numerical errors in the phase diagram are calculated as follows. The quantity βK_{xy} varies linearly with η at all potential strengths. Therefore the numerical error in η is proportional to the error in βK_{xy} (see Fig. 9). Using all these we obtain the RLIF phase diagram for hard disk systems (Fig.10).

Further, comparing with previous computations[22,23] of the phase diagram for this system (also shown in Fig. 10) we find that, within error- bars, our results agree at all values of η and βV_0 with the results of W. Strepp *et. al.*[23]. Whereas, in numerical details, they disagree with the results of C. Das *et. al.*[22], though even these results show RLIF and are in qualitative agreement with ours. This validates both our method and the quantitative predictions of Ref.[28]. The effect of higher order terms in determining non-universal quantities has been pointed out earlier[2] for the planar rotor model but in the present case their inclusion appears to be crucial. Nevertheless, we expect our procedure to break down in the $\beta V_0 \to 0$ limit where effects due to the cross-over from a KT to a KTHNY[11,12] transition at $\beta V_0 = 0$ become significant. Indeed, as is evident from Fig. 3 for $\beta V_0 < 1$ the dislocation probabilities of both type I and type II dislocations are similar[48] and the assumptions of FNR theory and our process (which involves only type I dis-

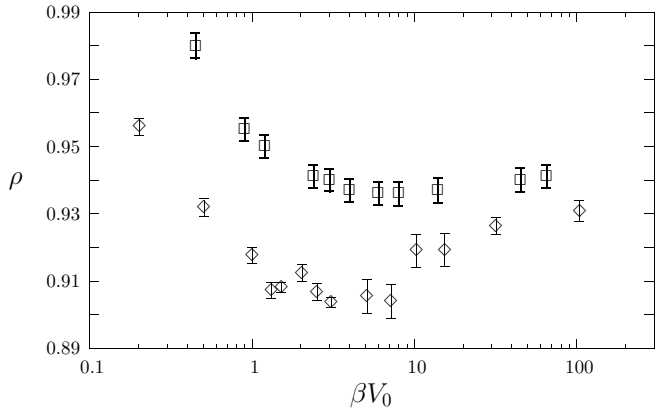

FIG. 11: Phase diagram for soft disks: □ denote our calculation, ◇ indicate earlier simulation data[25,26]. The vertical lines are the error- bars.

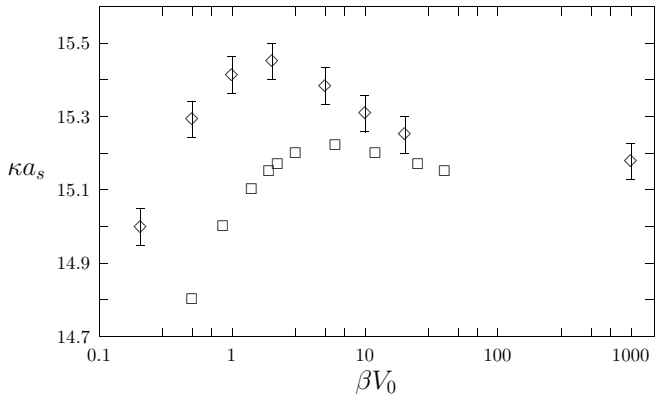

FIG. 12: Phase diagram for particles interacting via the DLVO potential. □ denote our calculation, ◇ show the earlier simulation data[24]. The vertical lines are the error- bars. Error bars in our calculation being smaller than the symbol size are not shown.

locations) need not be valid at small potential strengths. This fact is also supported by Ref.[23] where it was shown that though at $\beta V_0 = 1000$ the scaling of susceptibility and order parameter cumulants gave good data collapse with values of critical exponents close to FNR predictions, at $\beta V_0 = .5$, on the other hand, ordinary critical scaling gave better data collapse than the KT scaling form, perhaps due to the above mentioned crossover effects. In the asymptotic limit of $\beta V_0 \to \infty$ the system freezes above $\eta = .706$ which was determined from a separate simulation in that limit. This number is very close to the earlier value $\eta \sim .71$ quoted in Ref.[23]. As expected, the freezing density in the $\beta V_0 \to \infty$ limit is lower than the value without the periodic potential *i.e.* $\eta \simeq .715$.

In a similar fashion it is possible to find out phase diagrams of any 2-d system in presence of external modulating potential commensurate with the density of the system. We illustrate this by calculating similar phase diagrams for two other systems, viz. soft disks and the DLVO system. The soft disks interact via the potential :

$$\phi(r) = \frac{1}{r^{12}}$$

where r denotes the separation between particles. In simulations, the cutoff distance is chosen to be $r_c = 2$ above which the particles are assumed to be non- interacting. Apart from the external potential strength βV_0 the relevant thermodynamic quantity is the number density $\rho = N/L_x L_y$. In finding 'bare' elastic moduli from restricted simulations the stress is calculated from the Eq.7. As this expression does not involve any Dirac delta functions unlike the case of hard disks, we do not require any fitting like Figs.4,6 to obtain the stresses. The elastic moduli are again found from stress- strain curves like Figs.5,7. The dislocation fugacity of type I is calculated from rejection ratio of dislocation generating moves. All these, at a given ρ value generate the initial conditions x_0' and y_0' in RG flow diagrams. The crossing of these initial conditions with the separatrix found from Eq.2 gives the phase transition points. The phase diagram is plotted and compared with phase diagram from earlier simulations[25,26] in Fig.11. The error bar in ρ is found from the error in K_{xy}, as K_{xy} varies linearly with ρ, through the relation $\delta\rho/\rho = |1 + a/\rho b|(\delta K_{xy}/K_{xy})$. The quantities a and b are found from linear fitting (of form $a + bx$) of K_{xy} vs. ρ curve, at any given βV_0. The phase diagram (Fig. 11) again clearly shows reentrance (RLIF). This is in qualitative agreement with earlier simulations[25,26] (see Fig.11).

For charge stabilized colloids the inter-particle potential that operates is approximately given by the DLVO potential[39,40]:

$$\phi(r) = \frac{(Z^* e)^2}{4\pi\epsilon_0\epsilon_r}\left(\frac{exp(.5\kappa \mathrm{d})}{1 + .5\kappa \mathrm{d}}\right)^2 \frac{exp(-\kappa r)}{r}$$

where r is the separation between two particles, d is the diameter of the colloids, κ is the inverse Debye screening length, Z^* is the amount of effective surface charge and ϵ_r is the dielectric constant of the water in which the colloids are floating. In order to remain close to experimental situations and to be able to compare our phase diagram with the simulations of Strepp et. al.[23] we use $T = 293.15K$, d= $1.07\mu m$, $Z^* = 7800$, $\epsilon_r = 78$. In experiments, the dimensionless inverse Debye screening length κa_s can be varied either by changing κ through the change in counter-ion concentration or by changing a_s by varying density[49]. We perform the restricted Monte-Carlo simulation as described in section II. In simulations we vary κ and keep the particle spacing in ideal lattice $a_s = 2.52578\mu m$ (density) fixed. Further, we use a cut- off radius r_c such that, $\phi(r > r_c) = 0$ where r_c is found from the condition $\beta\phi(r_c) = .001$. We find out phase transition points (in κa_s) at different external potential strengths βV_0 in the same fashion as described earlier. The bare renormalizable quantities x_0'

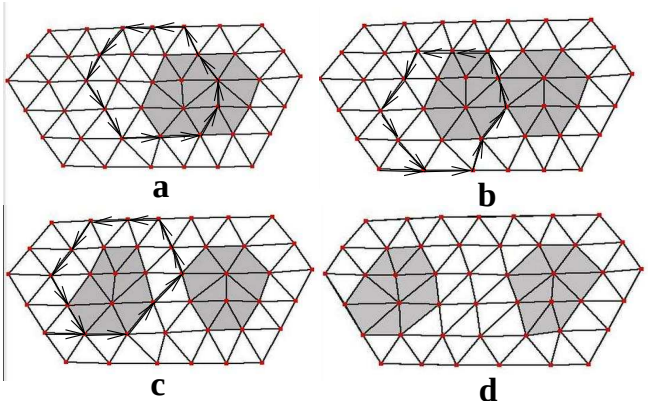

FIG. 13: The figures a – d which we have drawn using the applet "voroglide"[50] show four steps of separation of a type I dislocation pair, from a separation of a_0 to $4a_0$. The shaded regions show the $5-7$ disclination pairs constituting the dislocations. Burger's circuits are shown in a – c. Note that for separations $\geq 2a_0$ separate Burger's circuits around each disclination pair give rise to non-zero Burger's vectors, giving the dislocations their individual identity. This shows that the minimum meaningful separation between dislocation cores $r_{min} = 2a_0$.

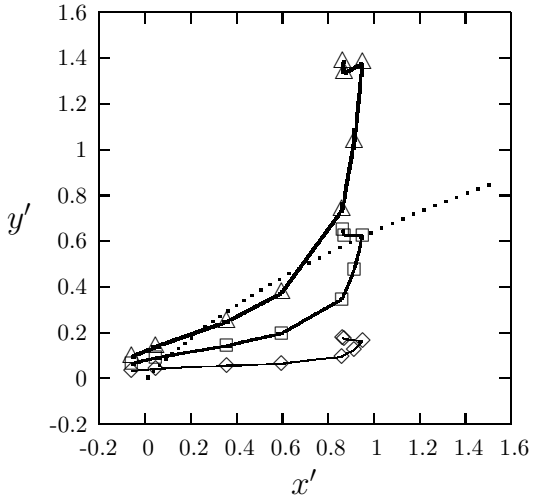

FIG. 14: Similar to Fig.8. The initial conditions x_0' and y_0' are plotted as a function of βV_0. The different data sets are created for different values of r_{min}. The symbols mean the following : $\diamond$ denotes data for $r_{min} = a_0$, $\square$ denotes that for $r_{min} = 2a_0$ and $\triangle$ denote data for $r_{min} = 3a_0$. The dotted line denotes the non- linear separatrix.

and y_0' are found from restricted Monte- Carlo simulations for various βV_0 at each κa_s. The phase transition points are calculated from the intersection of these initial conditions with the separatrix found from Eq.2. Thus we obtain the phase diagram in $\kappa a_s - \beta V_0$ plane (Fig. 12). βK_{xy} varies linearly with κa_s and the error in K_{xy} generates the error in κa_s (Fig.12) through the relation $\delta(\kappa a_s)/(\kappa a_s) = |1 + a/b\kappa a_s|(\delta K_{xy}/K_{xy})$. The quantities a and b are found from linear fitting (of form $a + bx$) of K_{xy} vs. κa_s curve, at any given βV_0. Though there is a quantitative mismatch between our data and that of Strepp *et. al.*[24], our data shows a clear region in κa_s (between 15.1 and 15.2) where we obtain re-entrance (RLIF). This is in contrast to the simulated phase diagram of C. Das *et. al.*[22], where they observe absence of re-entrance at high field strengths. We do not plot their data as the parameters these authors used are not the same as the ones used in Fig.12.

It is interesting to note that, with increase in range of two- body interaction potentials the depths of re-entrnace (in η, ρ or κa_s) decreases. This is again in agreement with the understanding that, the re-entrant melting comes about due to decoupling of the 1-d trapped layers of particles that reduces the effective dimensionality thereby increasing fluctuations. With the increase in range of the interacting potentials this decoupling gets more and more suppressed, thereby reducing the region of re-entrance.

One aspect of our study which stands out is the exceptionally better agreement of our results with previous simulations for hard disks as opposed to systems with soft potentials like the soft disks and the DLVO. This could, in principle, be due either (a) to the failure of the RG equations used by us or some other assumptions in our calculations (b) or to unaccounted finite size effects in earlier simulations. While it is difficult to estimate the effect of (a) since RG equations to higher orders in y are unknown at present, we may be able to motivate an estimation for (b). In order to explain the discrepancy in the positions of the phase boundaries, we need to go into some details of how the phase diagrams were obtained in the earlier simulations. In these simulations[23,24,25,26] the phase boundaries were obtained from the crossing of the order parameter cumulants[30,31] for various coarse graining sizes. The system sizes simulated in these studies are the same ($N = 1024$). However, the range of interaction differs. To obtain an objective measure we define the range of the potentials ξ as that at which the interaction potential ϕ is only 1% of its value at the lattice parameter. In units of lattice parameter, we obtain, for soft disks $\xi = 1.47$ and for the DLVO potential $\xi = 1.29$ at typical screening of $\kappa a_s = 15$. By definition, for hard disks $\xi = 1$. The particles within the range of the potential are highly correlated and we calculate the number N_{corr} of such independent bare *uncorrelated particles* within the full system size. N_{corr} takes the values $N_{corr} = 1024,\ 473.88,\ 615.35$ for hard disks, soft disks and the DLVO potential respectively. Since the effective system sizes are smaller for the soft potentials, finite size effects are expected to be larger. In this connection, it is of interest to note that in the same publications[23,24,25,26] a systematic finite size analysis showed that the phase diagrams shift towards higher (lower) density (kappa) for hard and soft disks (DLVO). A look at Fig.11 and 12 should convince the reader that such a shift would ac-

tually make the agreement with our results better. We emphasize here that our present restricted simulations are virtually free of finite size effects since the system does not undergo any phase transition.

Before we end this section, we discuss the reasons behind the particular choice of r_{min} that we made throughout this manuscript. In practice, it is possible to give individual identification to a dislocation only when Burger's vector separation within a pair is $\geq 2a_0$ (Fig.13) *i.e.* $r_{min} = 2a_0$. For $r \geq 2a_0$ Burger's loops can be drawn around each $5-7$ disclination pair (Fig.13) giving rise to a non-zero Burger's vector. In unrestricted simulations and in experimental situations after a disclination quartet is formed, they get separated out and the easy direction of separation is the glide direction which is parallel to the Burger's vector. In Fig.13 we show four steps of separation of such a dislocation pair of type I. After motivating $r_{min} = 2a_0$ we show, in Fig.14, the three sets of initial values corresponding to $r_{min} = a_0,\ 2a_0,\ 3a_0$ along with the non-linear separatrix at $\eta = .7029$ of hard disk system. $r_{min} = a_0$ predicts the system to be in solid phase for any arbitrarily small amount of external potential and to melt at larger βV_0. This behaviour contradicts physical expectation that the melting density at $\beta V_0 = 0$ has to be larger than that at $\beta V_0 = \infty$. On the other hand, while $r_{min} = 3a_0$ does not produce any unphysical prediction, it shrinks the region of re-entrance in the βV_0 direction. Therefore $r_{min} = 2a_0$ is the minimum value for r_{min} that could be chosen to produce physically meaningful results and this choice remains in closest agreement with simulation data.

IV. CONCLUSION

We have presented a complete numerical renormalization group scheme to calculate phase diagrams for 2-d systems under a commensurate modulating potential. We have used FNR theory along with this scheme to calculate phase diagrams for three different systems, namely, the hard disks, the DLVO and the soft disks. In all the cases we have found laser induced freezing followed by a re-entrant laser induced melting. We show that the re-entrance behavior is built into the 'bare' quantities themselves. We find extremely good agreement with earlier simulation results. In particular the phase diagram for hard disk comes out to be exactly the same as found from one set of earlier simulations[23].To obtain the correct phase diagram, however, flow equations need to be correct at least upto next to leading order terms in the dislocation fugacity. Our results, especially for small potential strengths, is particularly sensitive to these terms. Cross-over effects from zero potential KTHNY melting transition are also substantial at small values of the potential.

Acknowledgments

The authors thank Peter Nielaba, Wolfram Strepp, Abhishek Chaudhuri, Erwin Frey, Abhishek Dhar, Madan Rao and Yacov Kantor for useful discussions; D. C. thanks C.S.I.R., India, for a fellowship. Financial support by DST grant SP/S2/M-20/2001 is gratefully acknowledged.

[1] J. M. Kosterlitz and Thouless, J. Phys. C **6**, 1181 (1973).
[2] S. Sengupta, P. Nielaba, and K. Binder, Europhys. Lett. **50**, 668 (2000).
[3] S. Sengupta, P. Nielaba, and K. Binder, Phys. Rev. E **61**, 6294 (2000).
[4] M. S. Rzchowski, S. P. Benz, M. Tinkham, and C. J. Lobb, Phys. Rev. B **42**, 2041 (1990).
[5] S. N. Coppersmith *et al.*, Phys. Rev. Lett. **46**, 549 (1981).
[6] A. Chowdhury, B. J. Ackerson, and N. A. Clark, Phys. Rev. Lett. **55**, 833 (1985).
[7] Q.-H. Wei, C. Bechinger, D. Rudhardt, and P. Leiderer, Phys. Rev. Lett. **81**, 2606 (1998).
[8] F. Huang, M. T. Kief, G. J. Mankey, and R. F. Willis, Phys. Rev. B **49**, 39623971 (1994).
[9] W. Durr *et al.*, Phys. Rev. Lett. **62**, 206209 (1989).
[10] *Ordering in Two Dimensions*, edited by S. K. Sinha (North-Holland, Amsterdam, 1980).
[11] D. R. Nelson and B. I. Halperin, Phys. Rev. B **19**, 2457 (1979).
[12] A. P. Young, Phys. Rev. B **19**, 1855 (1979).
[13] K. J. Strandburg, Phys. Rev. B **34**, 3536 (1986).
[14] D. R. Nelson, in *Phase Transitions and Critical Phenomena*, edited by C. Domb and J. Lebowitz (Academic Press, New York, 1983), Vol. 7, p. 1.
[15] M. S. S. Challa and D. P. Landau, Phys. Rev. B **33**, 437 (1986).
[16] A. Zippelius, B. I. Halperin, and D. R. Nelson, Phys. Rev. B **22**, 2514 (1980).
[17] D. Chaudhuri and S. Sengupta, Europhys. Lett. **67**, 814 (2004).
[18] D. Chaudhuri and S. Sengupta, Europhys. Lett. **68**, 160 (2004).
[19] J. Chakraborti, H. R. Krishnamurthy, A. K. Sood, and S. Sengupta, Phys. Rev. Lett. **75**, 2232 (1995).
[20] C. Das and H. R. Krishnamurthy, Phys. Rev. B **58**, R5889 (1998).

[21] C. Das, A. K. Sood, and H. R. Krishnamurthy, Physica **A 270**, 237 (1999).

[22] C. Das, P. Chaudhuri, A. K. Sood, and H. R. Krishnamurthy, Current Science **80**, 959 (2001).

[23] W. Strepp, S. Sengupta, and P. Nielaba, Phys. Rev. E **63**, 046106 (2001).

[24] W. Strepp, S. Sengupta, and P. Nielaba, Phys. Rev. E **66**, 056109 (2002).

[25] W. Strepp, S. Sengupta, M. Lohrer, and P. Nielaba, Computer Physics Communications **147**, 370 (2002).

[26] W. Strepp, S. Sengupta, M. Lohrer, and P. Nielaba, Mathematics and Computers in Simulation **62**, 519 (2003).

[27] J. Chakraborti, H. R. Krishnamurthy, and A. K. Sood, Phys. Rev. Lett. **73**, 2923 (1994).

[28] E. Frey, D. R. Nelson, and L. Radzihovsky, Phys. Rev. Lett. **83**, 2977 (1999).

[29] I. W. Hamley, *Introduction to Soft Matter: polymer, colloids, amphiphiles and liquid crystals* (Wiley, Cluchester, 2000).

[30] K. Binder, Phys. Rev. Lett. **47**, 693 (1981).

[31] D. P. Landau and K. Binder, *A Guide to Monte Carlo Simulations in Statistical Physics* (Cambridge University Press,, Cambridge, UK, 2000).

[32] A. Jaster, Physica A **277**, 106 (2000).

[33] D. S. Fisher, B. I. Halperin, and R. Morf, Phys. Rev. B **20**, 4692 (1979).

[34] D. J. Amit, Y. Y. Goldschmidt, and G. Grinstein, J. Phys. A: Math. Gen. **13**, 585 (1980).

[35] This assumption is similar in spirit to assuming that a particle which reaches the saddle point in the Kramers barrier crossing problem would automatically cross the barrier[51] .

[36] Note that the calculation of the bare fugacity from the dislocation probability is, we believe, more accurate that the procedure used in[17] .

[37] O. Farago and Y. Kantor, Phys. Rev. E **61**, 2478 (2000).

[38] In the presence of an external 1D modulating potential periodic in the y- direction the stress has contribution from another virial- like additive term, $-\frac{\beta \mathrm{d}^2}{S}\left\langle \sum_\lambda y^\lambda f_y^\lambda \right\rangle$, where y^λ is the y-component of position vector of particle λ. This contribution comes from the part of the free energy that involves higher energy (massive) excitations. For the elastic free energy which is lowest order in the displacement gradient (Eq.1) this part does not contribute towards the elastic constants, as the x- and y- component of gradient remain uncoupled. This extra term in stress remains a constant background without disturbing the elastic constants connected to the Young and shear modulus that corresponds to distortions of the system in the low energy directions. We therefore neglect this background in calculating stresses where from we obtain the elastic moduli. .

[39] E. J. W. Verwey and Overbeek, *Theory of Stability of Lyophobic Colloids* (Elsevier, Netherlands, 1948).

[40] Derjaguin, B. V., Landau, and L. D., Acta Phys. Chim., USSR **14**, 633 (1941).

[41] B. Alder and T. Wainwright, Phys. Rev. **127**, 359 (1962).

[42] J. Zollweg, G. Chester, and P. Leung, Phys. Rev. B **39**, 9518 (1989).

[43] H. Weber and D. Marx, Europhys. Lett. **27**, 593 (1994).

[44] V. Ryzhov and E. Tareyeva, Phys. Rev. B **51**, 8789 (1995).

[45] J. P. Hansen and I. R. MacDonald, *Theory of simple liquids* (Wiley, Cluchester, 1989).

[46] This interaction in colloids is due to polarization of the dielectric colloidal particles by the electric field of the laser. Though experiments of Refs.[6,7] use charged colloids, the interaction of hard sphere colloids with lasers is similar .

[47] D. Frenkel and B. Smith, *Understanding Molecular Simulation*, 2nd ed. (Academic Press, New York, 2002).

[48] In analysing Fig.3 we must keep in mind that we can calculate from our simulations only the probability of formation of a disclination quartet. While we can, perhaps, safely assume that if type I dislocations are involved, they will seperate out with unit probability, the same can not be said of type II dislocations. This means that the probability of type II dislocations could be much lower than what Fig.3 suggests. .

[49] C. Bechinger and E. Frey, J. Phys.: Condens. Matter **13**, R321 (2001).

[50] http://www.pi6.fernuni-hagen.de/GeomLab/VoroGlide/index.html.en .

[51] H. A. Kramers, Physica **7**, 284 (1940).